On the fretting fatigue crack nucleation of complete, almost complete and incomplete contacts using an asymptotic method

Pierre Panico, Thibaut Chaise, Marie-Christine Baietto, Nicolas Guillemot, Cédric Poupon

On the fretting fatigue crack nucleation of complete, almost complete and incomplete contacts using an asymptotic method

Pierre Panico [1,2], Thibaut Chaise[1*], Marie-Christine Baietto[1], Nicolas Guillemot[2], Cédric Poupon[3]

[1] Univ Lyon, INSA Lyon, CNRS, LaMCoS, UMR 5259, 69621 Villeurbanne, France

[2] Airbus Helicopters, Aéroport Marseille/Provence 13725 Marignane Cedex, France

[3] Airbus Commercial Aircraft, Material and Processes Laboratory, D41 Rue Marius Terce, 31300 Toulouse, France

Corresponding author Thibaut Chaise: email thibaut.chaise@insa-lyon.fr

1. Abstract

In this work, the fretting crack nucleation of an aeronautical Ti-10V-2Fe-3Al titanium alloy is investigated. The main difficulty when designing complex industrial systems, especially helicopters rotor parts, lies in the prediction of the assembly interfaces behaviour. Those areas can be subjected to fretting loading characterized by a very confined multiaxial high stress gradient, leading to fatigue crack nucleation. This kind of failure reduces the parts potential lifetime and increases therefore the security margin that can be considered.

The aim of this paper is to provide a criterion to prevent crack nucleation on industrial contacts configurations. To reach this objective, this study focuses on the geometrical conditions, loadings and material properties linked to crack initiation. Two dedicated fretting test campaigns are used to study crack initiation conditions with various contact shapes and loadings on the same material. The crack initiation conditions are compared with a contact mechanics representation based on asymptotic methods. This method allows the stress field evaluation at the hot spot location by using the problem's eigenvalues.

The combination of the asymptotic method with contact mechanics and the Goodman approach allows to represent the key parameters of the fretting fatigue crack initiation. They include the impacted material volume, the shear intensity and the bulk

stress. A fretting fatigue crack initiation criterion is proposed. It is based on classical material properties and the bulk stress ratio R_{σ_0} only and is applicable to all sorts of contact shapes. The main interests of this prediction method are the absence of size effect parameters for industrial contacts and its efficiency, as it is only based on analytical formulations.

2. Nomenclature

P	Normal contact load
Q	Tangential contact load
σ_0	Bulk stress
P_0	Maximum contact pressure (Cylindrical pads)
P_{mean}	Mean contact pressure (plane pads)
$P_0{}^{ref}$	Pressure scaling value
R	Geometry radius
R_a	Arithmetic mean roughness
R_{σ_0}	Bulk stress Load ratio, $R_{\sigma_0} = \dfrac{\sigma_{0\,min}}{\sigma_{0\,max}}$
R_Q	Tangential load ratio $R_Q = \dfrac{Q_{min}}{Q_{max}}$
Q_{th}	Tangential contact load threshold leading to crack nucleation
f	Coefficient of friction
a	Contact half-width
b	Stick zone half-width
e	Stick zone offset
d	Slip zone size
σ_f	Endurance stress limit at 10^6 cycles, alternating bending tests
R_m	Ultimate Tensile strength
ΔK^{th}	Material crack propagation threshold
K_N	Normal stress intensity at the contact edge
K_T	Tangential stress intensity at the contact edge

ΔK^{eff}	Effective stress intensity factor range
ΔK_T^{th}	Tangential stress intensity crack nucleation threshold
$\Delta K_T^{th,PF}$	Plain fretting tangential stress intensity crack nucleation threshold
$\Delta K_T^{th,FF}$	Fretting fatigue tangential stress intensity crack nucleation threshold
σ_1	Maximum principal stress
σ_1^{max}	Maximum principal stress highest value on a loading cycle
$\sigma_1^{dyn}, \sigma_1^{stat}$	Alternating and constant component of the maximum principal stress describing a loading cycle

3. Intro

In a context of cost saving design and with the risk of unpredicted crack initiation in critical structures, the helicopters industry is looking deeply in the field of fretting failure prediction, a contact induced fatigue crack phenomenon. By proposing fretting free solutions, the goal is to increase safety, maintainability and robustness of the designs.

Fretting is a damaging phenomenon associated with small displacements between two contacting bodies and a large number of fatigue cycles. Tangential loaded Hertzian contacts are usually divided into three groups depending on the displacement amplitude (Vincent, et al., 1992) : gross slip regime - the two bodies present a relative motion, the partial slip regime - where a stick zone remains and the mixed slip regime – where some cycles are in partial slip configuration and others in gross slip. The dominant damaging phenomenon under fretting is strongly linked to those slipping regimes as proposed by Blanchard et al. (Blanchard, 1991). The gross slip regime is leading to wear, the partial slip regime to crack nucleation whereas the mixed mode regime has a combined response between wear and crack initiation.

The fretting risk in industrial contacts occurs mainly in rotor parts, where a constant load – the centrifugal force – induces a pre-load on the contact and an alternating load – blade flapping moment or pitch load – induces small displacements at the contact interface. The shapes of these contacts are mostly chamfered edge parts on

a plane. In this work the chamfer has not been considered by assuming that the main impact on fretting crack nucleation is the presence of the sharp edge and not the contact edge angle. From (Churchman, et al., 2006) and (Karuppanan, et al., 2008) it can be inferred that the major influence of a chamfer angle on the contact behaviour is on the coefficient of friction preventing the pad from gross slip.

An industrial contact submitted to fretting can be schematically represented as a pad pressed in contact with a plane by a normal load P, see Figure 1. The plane can be subjected to a bulk stress, σ_0, and a tangential displacement, δ, is applied to the pad. The reaction force to this tangential displacement, Q, and the presence of an alternating bulk stress, generate shear stresses at the contact interface. To decompose the influence of these loadings different tests are performed: so-called plain fretting tests, where only a tangential displacement is applied; and fretting fatigue tests where tangential displacement is combined with an alternating bulk stress.

Depending on the pad geometry, three contact cases can be observed and will be studied, (Hills, et al., 2017). A complete contact, see Figure 1 (a), is obtained when the pad presents sharp edges, as most industrial contacts. The contact size is equal to $2a$ and is independent of the normal load. The presence of sharp edges leads to a singular stress field at the contact edges. In the second case, rounded geometries lead to incomplete contacts, see Figure 1 (b-c). The size of incomplete contacts varies with the normal load. The stress field at the contact edges is then bounded. The contact configuration shown in Figure 1 (b) can be considered as an almost complete contact. It is composed of a square pad with tiny radii at the edges and behaves mainly as a complete contact except around the contact edges. Cylindrical contacts, Figure 1 (c), are the most used in laboratory tests but also the most different from the industrial application.

In each representation of Figure 1, an idealized stress distribution at the contact interface is presented. The red line corresponds to the contact pressure, or σ_{yy} in the contact local axis, which origin is at the contact centre. The blue line shows the shear stress distribution at the contact interface, or σ_{xy}. The shear stress distribution resulting from fretting forces is specific to partial slip contacts. It is highly dependent

on the tangential loading, the alternating part of the bulk stress and the Amontons-Coulomb friction coefficient.
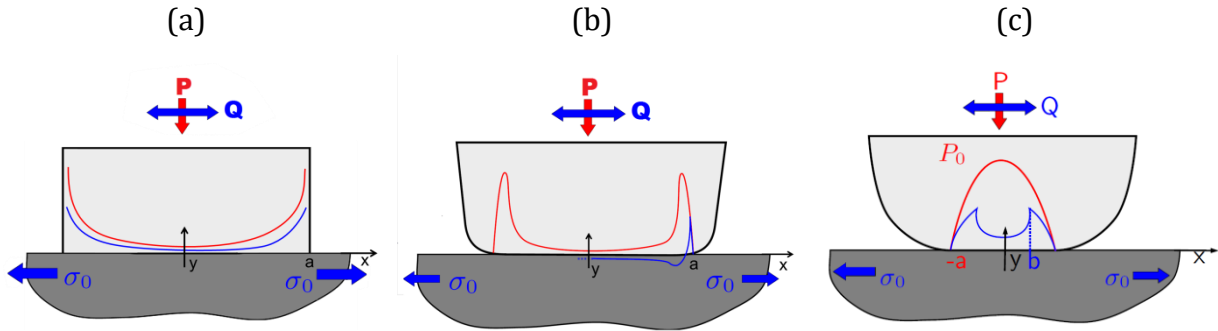

Figure 1: Complete, almost complete and incomplete contact subjected to a normal load P, a tangential load Q and a bulk stress σ_0. Schematic representations of the pressure (red) and shear (blue) at the contact interface for the maximum tangential load are indicated.

Several ways to predict fretting cracks nucleation have been proposed in the literature. Most of them rely on high accuracy contact mechanics models and classical fatigue criteria. Those models can be analytical (Hills, 1993), semi analytical or using finite element simulation (Baietto, et al., 2010). In each case the spatial discretization in the contact area must be sufficiently refined to compute continuous stress fields. It becomes then possible to estimate the hot spot location. The lifetime of the part subject to fretting fatigue can then be computed from a stabilized fatigue cycle with a fatigue criterion. The most commonly used when dealing with fretting topics are: the Crossland criterion (Ferre, et al., 2013), the Smith-Watson-Topper criterion (Proudhon, et al., 2005) (Fridrici, et al., 2005) or the Dang Van Criterion (Baietto, et al., 2013) (Fouvry, et al., 1996).

The size effect induced by the sharp stress gradient at the contact trailing edge prevents the direct prediction of fretting crack nucleation. A calibration process is therefore necessary. To be predictive while staying consistent with the hypotheses of homogeneous and isotropic materials, some methods have been developed to calibrate this stress gradient effect. The most common ways of calibrations are the critical point, line, and volume (Proudhon, et al., 2005) (Fridrici, et al., 2005) (Fouvry, et al., 1998) or the weight functions (Papadopoulos, 1996) (Hérédia, et al., 2014) (Amargier, 2011) methods. Depending on the authors, the calibration method is either a function of the stress field (Proudhon, et al., 2005) or of the materials' microstructure (Fouvry, et al., 1998) (Fridrici, et al., 2005). Those methods have shown their efficiency but are complex to integrate into industrial processes,

5

(Hérédia, et al., 2014). Among the drawbacks, one can cite the need for experimental results in the exact conditions of failure, the necessity of a dedicated model of the contact area and a heavy calibration process. Those methods are strongly dependent on the volume subjected to high stress. To bypass the spatial calibration of a fatigue criteria other methods have been investigated. They lie on the use of stress intensity factors to describe the spatial stress distribution and its magnitude.

The surrounding of a crack, in the framework of linear elastic fracture mechanics, and the stress distribution at a sharp edge contact both exhibit a stress singularity. The analogy between a crack and the contact edge has first been shown by Giannakopoulos and Suresh (Giannakopoulos, et al., 1998).

The fundamental concept behind this analogy is that a full description of the phenomenon at the interface is not necessary. An asymptotic description of the contact stress field can be used to reveal the eigenvalues of the contact edge as performed with the stress intensity factors on fracture mechanics. Those asymptotic parameters are useful to describe the contact slipping behaviour or the crack nucleation severity. They have been used to describe the presence of partial slip or separation at the edge of complete (Churchman, et al., 2006) (Karuppanan, et al., 2008) or incomplete contacts (Hills, et al., 2016) (Andresen, et al., 2019) by using the analogy with a notch or a crack.

Eigenvalues decomposition around the contact edge has also been used to describe the fretting crack nucleation severity in several complete contact cases (Flicek, et al., 2013) (Mugadu, et al., 2004) or incomplete contact cases (Naboulsi, 2005). A completely numerical determination of the contact edge eigenvalues has been developed by Montebello et al. using a 'Proper Orthogonal Decomposition' (Montebello, 2015). This description, based on a symmetric and an antisymmetric eigenvalues, shows a correlation with several fretting crack nucleation. Lately, Hills et al. used the asymptotic description at the contact edge from Dini et al. (Dini, et al., 2004) to analyse the incomplete contact fretting failure from two experimental campaigns on 2024-T351 aluminium alloy (Szolwinski, et al., 1998) (Nowell, 1988). This analysis highlights that one of the contact edge eigenvalues, the shear stress intensity factor ΔK_T, enables a good correlation between the different incomplete

contact experimental campaigns. A shear threshold is observed, below which no crack occurs (Hills, et al., 2017).

In this paper the contact trailing edge eigenvalues used by Hills *et al.*, K_N and ΔK_T are used to analyse fretting fatigue results from experimental campaigns on a Ti-10V-2Fe-3Al titanium alloy. A correlation between the contact edge eigenvalues and fretting crack nucleation experimental results is proposed. The asymptotic analyses of these experimental campaigns show a good correlation between crack initiation and contact mechanics, linear elastic fracture mechanics and fatigue. The contact mechanics framework is used to illustrate the relationship between the stress gradient and the different geometries through the parameter K_N. Using a linear elastic fracture mechanics analogy, fretting experimental results without bulk stress are correlated to the material's fatigue properties. Finally, the influence of the bulk stress is considered trough a Goodman relationship (Goodman, 1899). Those analogies lead to the proposal of a fretting crack nucleation prediction method. The proposed method can be used as a sizing criterion at 10^6 fatigue life cycles. It can be applied to several contact edge geometries and over a very wide range of loading ratios.

4. Experimental results

The purpose of this section is to provide experimental results for the developed model. Thresholds for fretting crack nucleation at 10^6 cycles for several contact geometries and load ratios have been determined. Those data have been obtained through two experimental campaigns called 'Incomplete Contact Fretting Nucleation' (ICFN) from (Hérédia, 2012) and (Hérédia, et al., 2014), and 'Almost Complete Contact Fretting Nucleation' (ACCFN) from the authors. The material studied in this work is the Ti-10V-2Fe-3Al titanium alloy, quenched and annealed. This material is mainly used in helicopters rotor applications because of its high fatigue performance.

The aim of the ICFN tests (Hérédia, et al., 2014) was to characterize the nucleation properties of the Ti-10V-2Fe-3Al both in plain fretting and fretting fatigue, i.e. without and with bulk stress, for contacts of cylindrical pads of various radii on plane samples. The experiments have been performed at LTDS laboratory, Ecole Centrale

7

de Lyon, France, using two different fretting tests set up. The ambition of ACCFN tests was to determine the crack nucleation occurrence in complete contacts configuration. This last geometry is more representative of industrial applications, especially in helicopter rotor parts and reveals the sharpest stress gradient at the contact edge. Those experiments have been performed at Airbus Commercial Aircraft, Material and Processes laboratory, Toulouse, France.

The geometries of the different pads used for the experiments are: four cylindrical pads with radii from $20\ mm$ to $80\ mm$; two rounded edge square pads with $0.5\ mm$ and $1\ mm$ radii and a sharp edge square pad. The flat part length of each of the square pads are respectively $9\ mm$, $8\ mm$ and $10\ mm$. The widths of all specimens, equal to $10\ mm$, is assumed sufficiently large to consider a plane strain hypothesis at their median axis. All the specimens have been polished and present an arithmetic mean roughness $Ra < 0.6\ \mu m$. The machining processes are considered to have a negligible influence on the fretting crack nucleation process of Ti-10V-2Fe-3Al as shown by (Hérédia, et al., 2011).

It has been shown on a similar alloy, that fretting crack nucleation is not reliant on loading frequency by Lykins et al. (Lykins, et al., 2001). The industrial application frequency range is $[4\ Hz; 20\ Hz]$, the experiments from Heredia *et al.* have been performed at $10\ Hz$ and our experiments at $15\ Hz$. These variations are considered as negligible.

The normal load, and therefore the contact pressure is kept constant along the 10^6 cycles to avoid any variation in the contact size. The maximum contact pressures P_0 of the cylindrical contacts are displayed in the Table 1 and Table 2. For all experiments, the tangential load varies from Q_{min} to Q_{max} with an alternate ratio $R_Q = -1$. The tangential load is normalized by the normal force applied during the test. The bulk stress σ_0, in the fretting fatigue experiments, is applied out of phase with the tangential loading to produce the most damaging configuration at the contact interface. The bulk stress ratios are $R_{\sigma_0} = 0.1$, $R_{\sigma_0} = 0.3$ or $R_{\sigma_0} = 0.8$ and the maximum bulk-stress values are different for all experiments.

8

4.1 Experimental set up

The plain fretting experimental results from Heredia et *al.* have been performed on a set-up where a reciprocating hydraulic cylinder is used to impose a displacement between the pad and the plane specimen. A constant normal load P is applied by a screw system. The normal force P, the imposed displacement δ, and the reaction force Q are recorded during the 10^6 cycles of the tests. Details on this test device can be found in (Kubiak, et al., 2005). The fretting fatigue experimental set-up is inspired by the dual actuators fretting fatigue test device from Fellows et al. (Fellows, et al., 1997) and Lee et al. (Lee, et al., 2006). The main advantage of this kind of test device is to allow desynchronised applications of the bulk stress and tangential displacement. Both tangential and bulk stress effort and displacements are recorded with the normal loads all along the test. Further details of this experimental test device can be found in (Meriaux, et al., 2010).

The experimental results from the ACCFN test campaign have been performed on an Airbus hydraulic test device, shown in Figure 2. This experimental set-up is composed by three hydraulic cylinders that allow applying the normal load, tangential displacement and bulk-stress independently. In Figure 2, the red and green parts are respectively the fretting pad and the plane dog bone specimen. The orange part fulfils two functions: it supports the plane specimen and applies the normal load. The blue part allows the relative tangential displacement between the pad and the plane.

This test device can be used into two configurations: plain fretting and fretting fatigue. In plain fretting configuration, $10\,mm$ thickness dog bone specimens are used as fretting specimen. The fretting fatigue loading is applied on a $2.8\,mm$ thickness dog bone specimen because of the bulk stress hydraulic cylinder capacity.
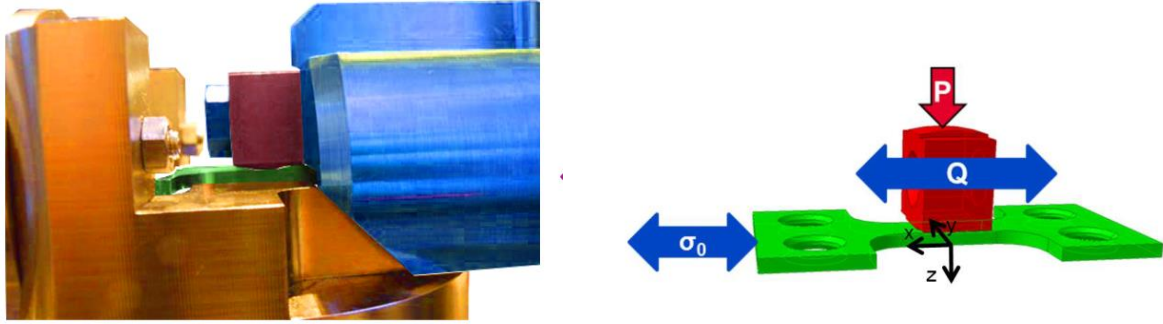
Figure 2 : Contact area on the Airbus device set-up: contact between the pad (red) and the plane specimen (green); support and normal load actuator (orange); tangential load actuator (blue)

One end of the plane specimen is clamped to the bulk stress hydraulic cylinder to apply the fretting fatigue loads whereas the other end is clamped to the support. A PTFE film is installed at the interface with the support when used in fretting fatigue conditions to apply a constant stress in the specimen depth and avoid any frictional stress diffusion in the support. The test bench has been calibrated to provide repeatable loads and avoid any normal load variations.

The alignment of the contacting planes is the main point for the representativeness of the complete contact. The cylinder on plane contacts are auto-adjusted thanks to their geometry and the presence of an hydrostatic bearing around the axis of the tangential force. The almost complete contacts have been calibrated to ensure the alignment. A comparison between this experimental set-up and the one used in plain fretting by Heredia *et al.* has been performed by Amargier *et al.* (Amargier, 2011) and illustrated a good correspondence in fretting crack nucleation results.

4.2 Fretting crack nucleation

All the tests presented in this paper were interrupted at 10^6 cycles and analysed to characterise the nucleation state at this fatigue life. The same procedure has been used in the different experimental campaigns. The specimens are cut perpendicularly to the fretting scar, which is equally distributed, far enough from the contact edge to ensure plane strain hypothesis. Those sections are coated and polished to measure the mean cracks depth, as shown in Figure 3 (b).

The observation of each specimen allows to determine a mean depth crack corresponding to the test parameters (geometry, normal load, tangential load and bulk stress).
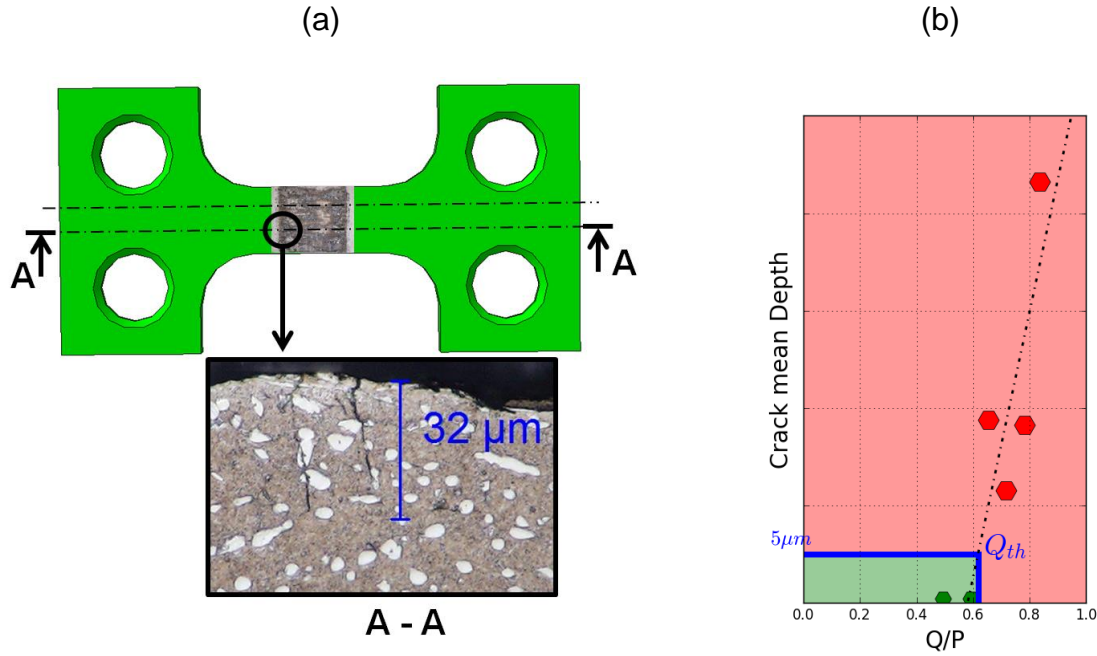
(a)   (b)

Figure 3 : Crack nucleation threshold determination: (a) crack depth measurement on cut and polished test specimen, (b) Q_{th} determination via mean crack depth.

The goal of those experiments is to find the tangential load, ΔQ, that produces the crack nucleation while keeping all other parameters constant. A few tests sharing the same experimental parameters are performed with several applied tangential displacements. Then the average crack depths for each test are used to determine the fictive tangential loading that would lead to a $5\ \mu m$ depth crack. This parameter is called the crack nucleation threshold Q_{th} as shown in Figure 3 (b). Three to eight fretting tests are therefore necessary to obtain a single threshold value. The crack length threshold of $5\ \mu m$ comes from the microscopic to mechanical short crack transition, (Tanaka, et al., 1981). The crack nucleation considered in this work is already a stage II crack, (Lamacq, et al., 1999). This crack, as shown on Figure 3 (b), is propagating with a 70° inclination from the surface, driven by the mechanical stress distribution through the grains.

All the nucleation thresholds with the corresponding experimental conditions are summarized in the following tables. Fretting crack nucleation thresholds from past studies, Table 1, are presented with the same scaling as in (Hérédia, et al., 2014). The maximum contact pressure P_0 is scaled by a scalar, $P_0^{\ ref}$. The maximum contact

11

pressures P_0 from these tests are in the interval $200\ MPa$ to $800\ MPa$. The maximum bulk-stress value is scaled by the material fatigue strength at 10^6 cycles, σ_f. The new experimental results, Table 2, are scaled with the same logic. As these configurations imply plane pads the local maximum pressure calculation is not widely admitted. The complete contact normal loading are therefore displayed as the mean pressure over the contact surface area, P_{mean}, scaled by $P_0{}^{ref}$.

Reference	Radius (mm)	$\dfrac{P_0}{P_0{}^{ref}}$	$\dfrac{\sigma_0{}^{max}}{\sigma_f}$	$\dfrac{Q_{th}}{P}$
R_{20}	20	1.36	0	0.6
R_{20}	20	1.57	0	0.45
R_{20}	20	1.76	0	0.41
R_{40}	40	1	0	0.79
R_{40}	40	1	0	0.72
R_{40}	40	1.5	0	0.43
R_{40}	40	1	0.07	0.63
R_{40}	40	1	0.13	0.45
R_{40}	40	1.5	0.13	0.26
R_{40}	40	1	0.27	0.22
R_{40}	40	1.5	0.27	0.14
R_{80}	80	1	0	0.61
R_{80}	80	1	0.07	0.44
R_{80}	80	1	0.13	0.33
R_{80}	80	1	0.27	0.14

Table 1: Fretting crack nucleation thresholds for incomplete contact (Hérédia, et al., 2014)

Reference	Radius	$\dfrac{P_{mean}}{P_0^{ref}}$	$\dfrac{P_0}{P_0^{ref}}$	$\dfrac{\sigma_0^{max}}{\sigma_f}$	$\dfrac{Q_{th}}{P}$
$R_{0.05}$	0	0.1	/	0	0.6
$R_{0.5}$	0.5	0.11	/	0	0.68
R_1	1	0.125	/	0	0.8
R_1	1	0.125	/	0.2	0.72
R_{30}	30	/	1.25	0	0.61
R_{30}	30	/	1.25	0.2	0.39

Table 2 : Fretting crack nucleation thresholds for almost complete and complete contact

All these data represent the boundary between the fretting safe conditions and the fretting crack nucleation conditions. These thresholds can therefore be used to establish a fretting crack criterion at 10^6 cycles.

5. Contact description

The loading conditions corresponding to crack nucleation observation are not self-sufficient to express a fretting crack nucleation criterion. Some authors have shown how the fatigue crack nucleation induced by fretting loads comes from the contact stress distribution at the interface (Lamacq, et al., 1997), (Fouvry, et al., 1996). The classical contact mechanics representation (Hills, 1993) is firstly used to study the contact conditions and the stress field.

Contact mechanics allow an efficient modelling of the stress field at the contact interface. An incomplete contact is considered uncoupled if both contacting parts are composed of elastically similar materials (Dundurs, 1969). In such a case, the normal contact can directly be solved using Hertz theory (Hertz, 1882). The partial slip produced by the tangential loading is described by the Mindlin and Cattaneo theory (Cattaneo, 1938) (Mindlin, 1949) and the influence of the bulk stress on the stick zone position following Hills *et al.* (Hills, et al., 1988). The coefficient of friction is here assumed to be constant at the contact interface. From consideration of the Amontons-Coulomb friction law at the macroscopic scale, the maximum tangential load Q is limited by the threshold imposed by the friction law, equation (1):

$$\frac{Q}{P} < f \tag{1}$$

The stress field in the specimen can be computed using the complex potential theory (Muskhelishvili, 1953). All the contributions can be concatenated in the case of an elastic behaviour following the Jäger-Ciavarella method (Jäger, 1997) (Ciavarella, 1998a) (Ciavarella, 1998b). This stress representation shows a high stress gradient at the trailing edge of the contact, as shown in Figure 4. The use of a fatigue criterion in this context has shown that this stress gradient is responsible of the crack nucleation in fatigue (Proudhon, et al., 2005) (Fridrici, et al., 2005) (Fouvry, et al., 1998).

The maximum value and shape of the stress field are strongly linked to the slip zone size, d. By using the contact mechanics formalism presented above, the σ_{xx} stress component at the trailing edge can be rewritten as Eq. (2), x being the tangential loading direction:

$$\sigma_{xx}(x, y = 0) = P_0 \sqrt{1 - \left(\frac{x}{a}\right)^2} + \frac{2fP_0}{a}\left(\sqrt{x^2 - a^2} - \sqrt{x^2 - (a-d)^2}\right) + \sigma_0 \tag{2}$$

$$d = a - b \pm e \tag{3}$$

with a the contact half width, b the stick zone half width and e the stick zone offset due to the bulk-stress.
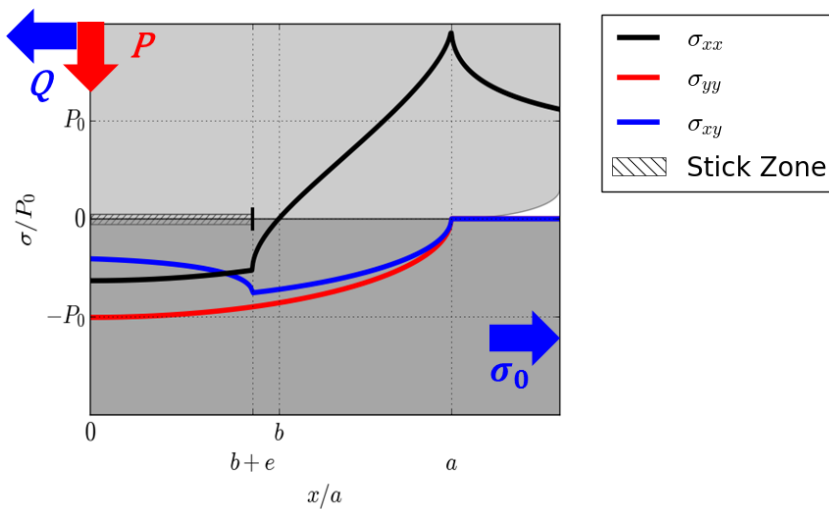

Figure 4 : Surfaces stresses at the trailing edge interface of a cylinder on plane contact

In Fig. 4, the plane strain stress components are plotted at the interface of a cylinder on plane contact subjected to fretting fatigue loading. This partial slip stress distribution at the contact edge shows a stick zone from 0 to $b + e$ and a partial slip zone from $b + e$ to a. In this partial slip zone, the shear stress is limited by the friction coefficient. The partial slip zone reveals a sharp stress gradient with a maximum value at the contact trailing edge.

It has been shown experimentally by different authors that the critical location is the contact edge or slightly inward the slip zone (Lamacq, et al., 1996), without any influence of the contact geometry (Hutson, et al., 2003) (Mall, et al., 2003). Our plain fretting and fretting fatigue experiments on the Ti-10V-2Fe-3Al material illustrates the same hot spot location as shown in Figure 5.
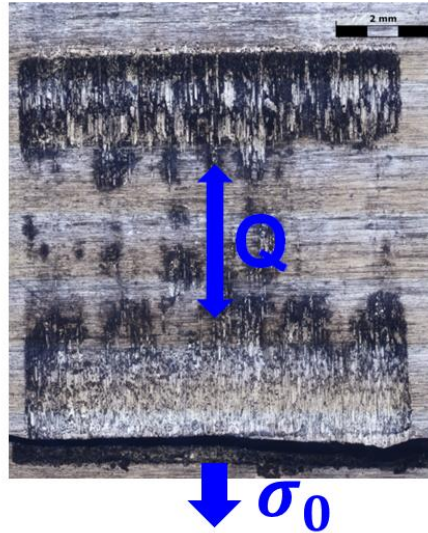

Figure 5 : Fretting fatigue scars for a rounded edge punch with a 1mm radius at 10^6 cycles.

Both contact mechanics analysis and experimental results show that the critical location is the contact edge (Ferre, et al., 2013), (Giannakopoulos, et al., 1998), (Hérédia, et al., 2014), (Proudhon, et al., 2005) (Fridrici, et al., 2005). To avoid a complex representation of the contact requiring a refined mesh, the idea is to use the contact eigenvalues at this location. An analytical formalism has been proposed by Dini et al. to describe the cylinder on plane contact (Dini, et al., 2004) and the rounded edge contact (Mugadu, et al., 2004) and will be recalled here.

5.1 Asymptotic Method definition

The description of the stress fields around the contact edge is performed with the contact edge eigenvalues: the intensity of the normal load K_N, and the intensity of the tangential load K_T. The asymptotic description uses two scalar coefficients that can be determined independently of one another.

5.1.1 Normal stress intensity

The concept is to shift the origin to the contact edge and to express the contact edge eigenvalue along the interface using the Newton's generalized binomial theorem on the analytical stress distribution. In this framework, the normal stress distribution around the contact edge is defined by Eq. (4):

$$\sigma_{yy} \simeq K_N \sqrt{s} \tag{4}$$

with K_N a scalar coefficient that represents the intensity of the normal stress field at the contact edge and s a local axis from the contact edge. The value of K_N is easily determined from Eq. (5) for a cylindrical pad contact (Hills, et al., 2016).

$$K_N = P_0 \sqrt{\frac{2}{a}} \tag{5}$$

The determination of K_N for a rounded edge pad can be done using only analytical equations from (Mugadu, et al., 2004) if the tangential loading Q is sufficiently small to avoid coupling effect. Otherwise the general method proposed by Fleury et al. (Fleury, et al., 2016) should be applied, where K_N can be described as:

$$\left(\frac{K_N \sqrt{R}}{E^*}\right)^3 = H_1 \left(\frac{-K_I}{E^* R^{1-\lambda_I}} + H \frac{K_{II}}{E^* R^{1-\lambda_{II}}}\right) \tag{6}$$

In this case the contact edge is defined as a notch. The stress field at the notch edge can be described by Williams asymptotic method (Williams, 1956) where λ_1 and λ_2 are the power orders of the singularity and K_I and K_{II} the mode I and mode II classical stress intensity factors. The bounded asymptotic coefficient K_N is then

determined with the pad radius, R, the equivalent elastic modulus of the contact E^* and the scalar coefficient H_1 and H computed by Fleury et al (Fleury, et al., 2016).

For a complete contact, the stresses are analytically not bounded at the edge. Physically, this discontinuity is not consistent, providing a straightforward application of the analytical results. After 10^6 cycles, the edges of several complete contacts have been measured and can be modelled as an almost complete with a radius $R = 0.05 \ mm$.

5.1.2 Tangential stress intensity

In a first approach, a shear stress scalar coefficient, consistent with a fully adhered contact, is determined:

$$\sigma_{xy} \simeq \frac{K_T}{\sqrt{s}} \tag{7}$$

The main advantage of this shear stress representation is that it is the same for all the contact configurations used in this work. K_T therefore represents the intensity of the tangential stress field at the contact edge and is composed of two terms. The first term depends on the tangential loading Q applied to the pad. The second is representative of the mismatch in strain when one of the contacting bodies is subjected to bulk-stress:

$$K_T = \pm \ \frac{Q}{\pi\sqrt{2a}} + \frac{\sigma_0}{4} \ \sqrt{\frac{a}{2}} \tag{8}$$

The sign of the first term depends on the contact edge considered. The local axis s, of the contact edge is directed inward the contact area and therefore can lead to a change in sign. The bulk-stress is assumed to be always directed outwards so that its influence on the shear stress is positive. More details on this point are presented in (Hills, et al., 2016).

The K_T parameter can be determined easily at each time step as long as the normal load is kept constant, avoiding any variation in the contact half width. In both

experimental campaigns, the normal load has been applied when the mean value of bulk-stress was constraining the plane specimen. So only the alternate part of the bulk-stress is producing shear stress at the contact interface.
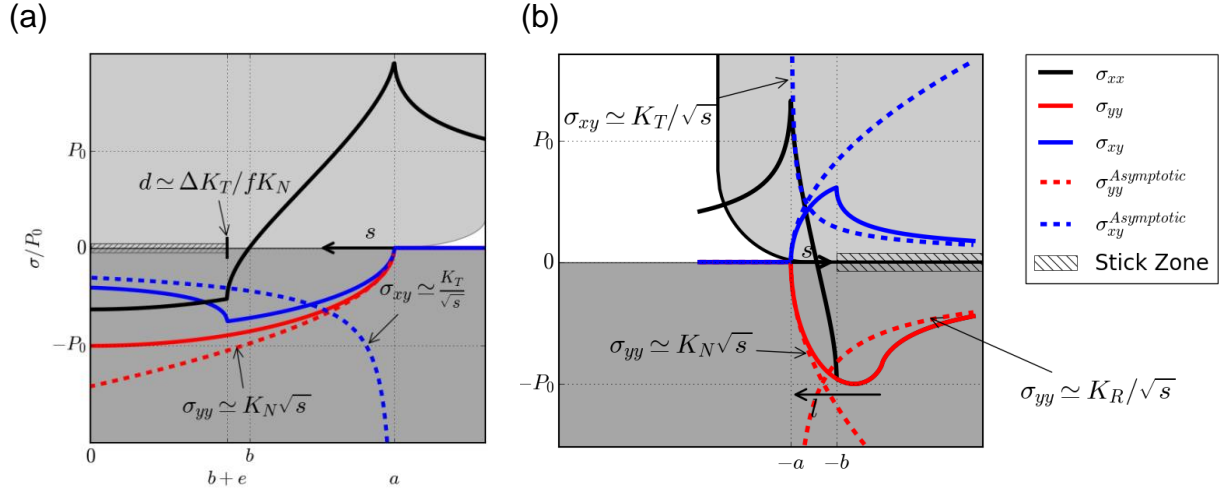
(a)

(b)

Figure 6 : Illustration of the asymptotic description at the trailing edge of the cylinder (a) and rounded edge pad (b) on plane contacts

Figure 6 represents the analytical stress distribution in plane strain condition for a cylinder on plane contact (a) and a rounded edge punch contact (b). A zoom on the trailing edge is made and the asymptotic stress distributions are shown in discontinuous lines. For cylinder on plane contacts, the bounded asymptotic parameter K_N and the singular asymptotic parameter K_T are sufficient to describe the contact edge area. For complete contacts, the singular pressure asymptotic parameter K_R can be added to describe the central part of the contact. This last parameter is not used in this study.

5.1.3 Asymptotic Fretting Map

All the fretting crack nucleation thresholds determined experimentally are here expressed through the asymptotic parameters to visualize the evolution of the shear intensity factor with the contact geometry and the presence of bulk-stress. Figure 7 represents the crack nucleation thresholds of the incomplete contact fretting nucleation and almost complete contact fretting nucleation in a $K_T \times K_N$ space. This enables an uncoupled representation of the crack nucleation thresholds depending on the normal load and shear stress intensity at the contact edge.

The following figures have been scaled with material sizing values. The experimental asymptotic shear values K_T are normalized by the crack propagation threshold in

shear mode $\Delta K_T{}^{th}$. The stress values are normalized by the fatigue strength at 10^6 cycles, σ_f, for alternate loads or by the ultimate tensile strength, R_m, for static loads.
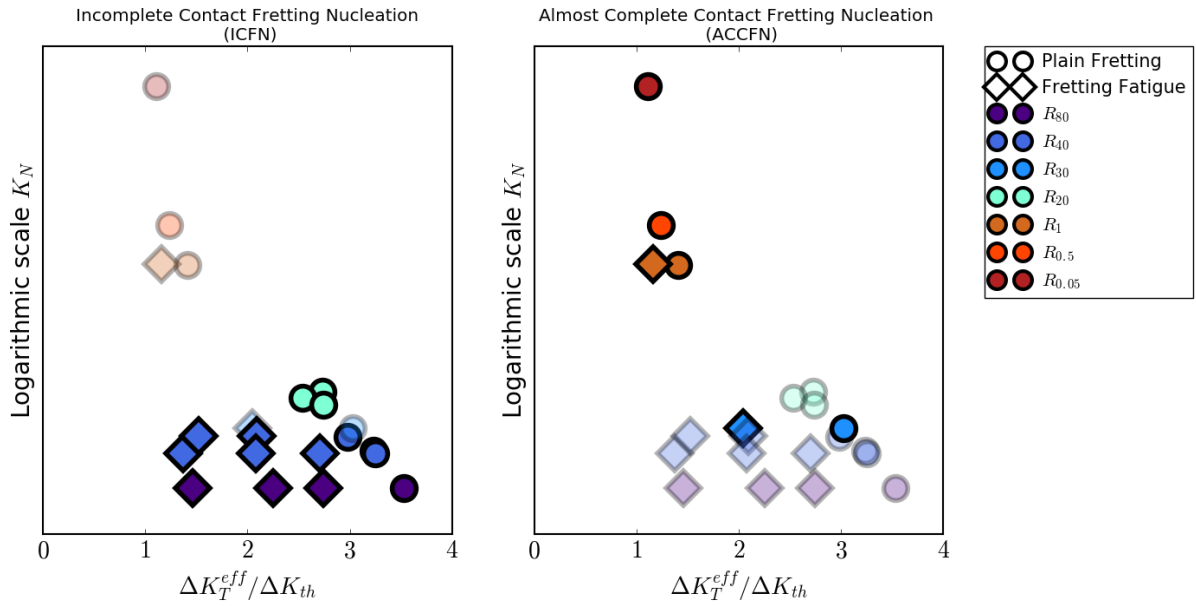

Figure 7 : Asymptotic fretting maps of both fretting test campaign at 10^6 cycles

The ICFN test campaign was focused on the characterisation of the bulk stress influence on cylinder vs plane configuration. The influence of various cylinder radii shows a decrease of the admissible shear intensity with smaller radii. In the meantime, the addition of a tensile bulk-stress produces a decrease of the admissible shear intensity factor at 10^6 cycles. The perturbation of the interface shear stress due to the bulk-stress is included in the K_T parameter.

The results from the ACCFN test campaign allow first to validate the similarity of the experimental test set ups used in the two campaigns. The thresholds obtained with the R_{30} cylindrical pad, with and without bulk stress, are here similar to those obtained by Heredia et al. (Hérédia, et al., 2014) in the ICFN campaign. Almost complete and complete contact geometries have been used from a $1\,mm$ radius to a sharp edge pad ($R_{0.05}$). The previous tendency is confirmed. The crack nucleation appears with a lower shear intensity parameter when the stress gradient increases. However, the influence of the bulk stress seems to be lower with rounded edge pads (R_1) than with cylindrical pads.

The admissible shear intensity factor is drastically decreasing with the evolution of the geometry towards the most singular ones. In the same way, each level of bulk

stress that has been applied decreases the shear intensity factor needed to nucleate a crack.

5.2 Asymptotic description properties

The asymptotic parameters can be used to determine various others properties of the contact, beyond the description of the stress fields at the crack nucleation hot spot. Due to their definition, they can either be compared to contact mechanics or to linear elastic fracture mechanics.

5.2.1 Contact mechanics analogies

It is possible to express several properties of the contact by substituting the eigenvalues at the contact edge into classical contact mechanics equations.

The gross slip condition, expressed from the Amontons-Coulomb friction law (Eq. (1)), can be expressed with the asymptotic parameters as in Eq. (9), with $d_{slip} > 1$ when the friction law is overcome.

$$d_{slip} = \frac{2\Delta K_T}{af K_N} \tag{9}$$

As discussed previously, the slipping zone size is strongly linked to the maximum value of the σ_{xx} stress distribution at the contact edge. By replacing the asymptotic parameters in the slip zone size equation, it becomes possible to express it like Eq. (10). Then by substituting it in Eq. (2) and using Newton's binomial theorem, an expression relying on K_N is obtained (equations (11) and (12)), and illustrated in Figure 8.

$$d = a\left(1 - \sqrt{1 - \frac{2\Delta K_T}{af K_N}}\right) \tag{10}$$

$$\sigma_{xx}(s > 0) \approx \sqrt{4f K_N \Delta K_T} + \sigma_0 - K_N\sqrt{s} - \frac{f K_N^2}{P_0} s \tag{11}$$

$$\sigma_{xx}(s < 0) \approx \sqrt{4f K_N \Delta K_T} + \sigma_0 - 2f K_N\sqrt{|s|} - \frac{f K_N^2}{P_0} s \tag{12}$$

The maximum value of the stress field at the trailing contact edge can be expressed with only the asymptotic parameters as shown in Eq. (13):

$$\sigma_{xx}{}^{max}(x = \pm a) = \sqrt{4fK_N\Delta K_T} + \sigma_0{}^{max} \qquad (13)$$

Eq. (13) shows the maximal stress at the trailing edge. The first term comes from the shear scalar coefficient range ΔK_T and is fully alternate. The second term is the maximum bulk stress in the specimen section, composed from a static, $\sigma_0{}^{stat}$, and an alternate load, $\sigma_0{}^{dyn}$.

At the trailing contact edge, σ_{xx} is the only stress component in plane strain conditions. Its value is then equivalent to the maximum principal stress at the contact edge:

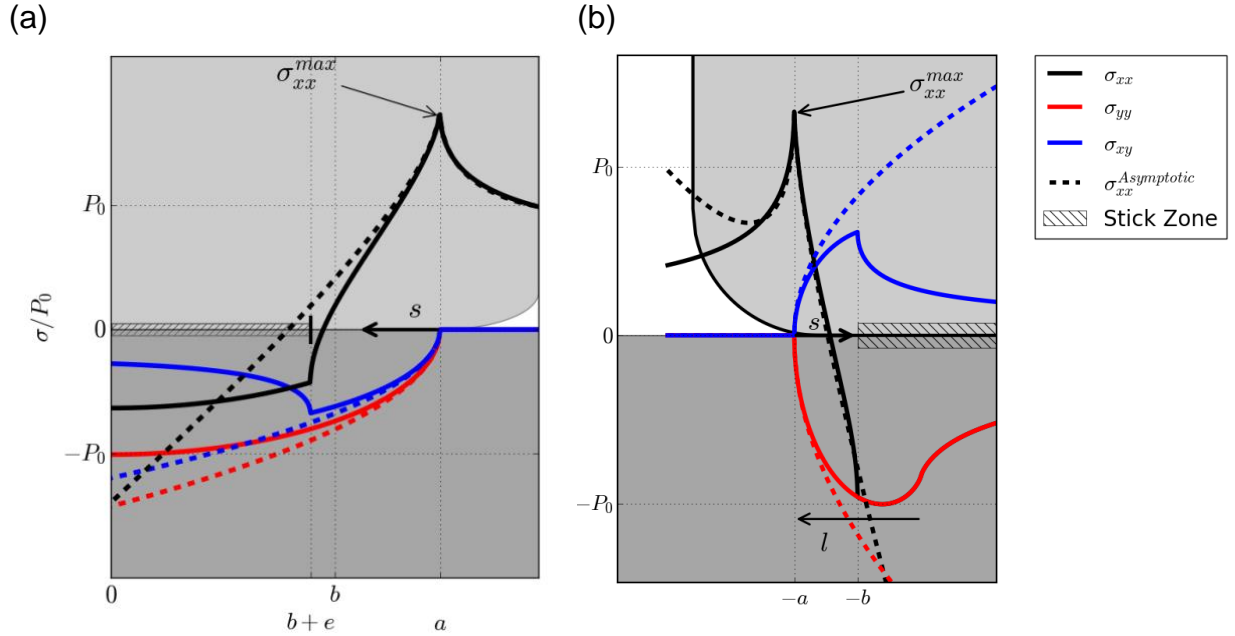$$\sigma_1{}^{max}(x = \pm a) = \sigma_{xx}{}^{max}(x = \pm a) \qquad (14)$$

(a) (b)

Figure 8 : Trailing edge stress gradient expressed with asymptotic parameters, (a) cylinder on plane trailing edge stresses, (b) rounded edge pad on plane trailing edge stresses

Equations (10) to (13) can be extended to a rounded edge contact by using the Jäger-Ciavarella theorem (Jäger, 1997) (Ciavarella, 1998a) (Ciavarella, 1998b) for both contacting geometries. The asymptotic description of the stress gradient at the trailing edge σ_{xx}, is in good accordance with the analytical stress gradient close enough to the contact edge. The maximum stress value at the trailing edge can be obtained from the normal stress intensity factor and the tangential stress intensity factor range with only one material parameter, the coefficient of friction.

From Eqs. (11) and (12) the shape of the stress gradient seems very dependent on the normal stress intensity factor K_N. This parameter encapsulates the amount of materials subject to high stress. It can therefore be used to replace the calibration step in the volume method to consider different kind of geometries that produce different kind of stress gradient at the trailing edge.
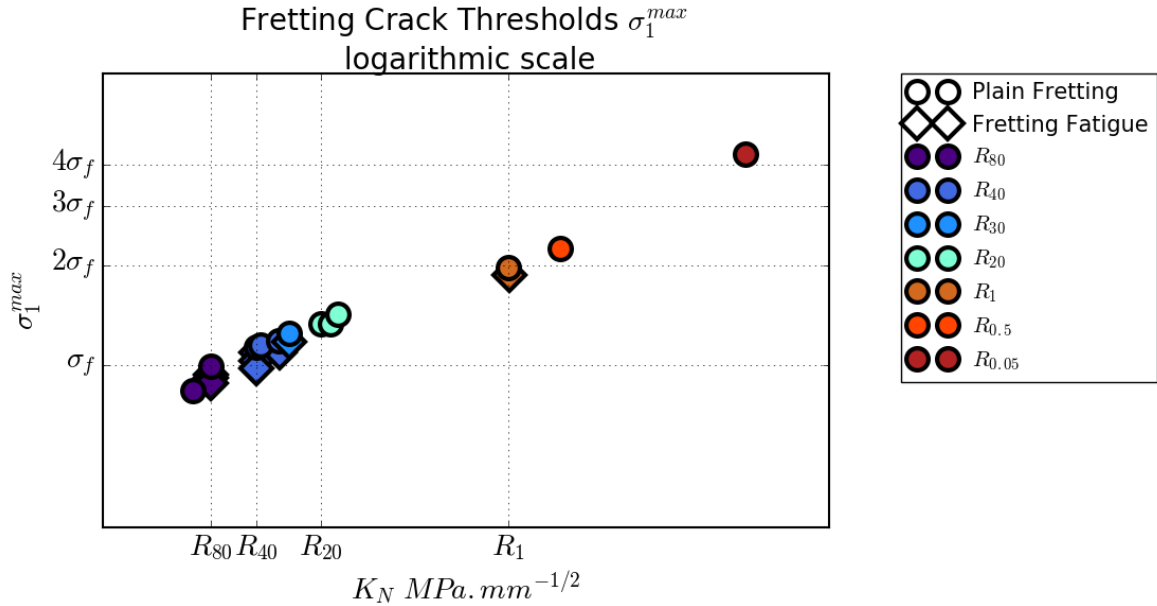

Figure 9 : Fretting crack nucleation thresholds maximum stress value vs. K_N parameter

The application of Eq. (13) at each crack nucleation thresholds shows values varying from σ_f to $4\sigma_f$ in Figure 9. The sharper the stress gradient the more important the maximum value is. A link appears between the material volume that is subjected to high stress and the crack nucleation. This behaviour has been observed by Papadopoulos et al. with plain fatigue experiments (Papadopoulos, 1996). When the stress is limited to a small area, the failure happens with higher stress values than standard fatigue limit because the presence of defects is statistically lower (Hild, 1992). This conclusion limits the use of local methods to evaluate the risk of fretting crack nucleation. A method including the stress diffusion in the bulk will therefore be used.

5.2.2 Linear Elastic Fracture Mechanics analogy

In linear elastic fracture mechanics, the local state of stress is meaningless to describe the severity of a notch or a pre-crack. The presence of the geometrical

discontinuity is included in the stress intensity factors. The stress field around the crack tip can then be computed using the stress intensity factors and the Williams series (Williams, 1956). This representation of the stress field takes its origin at the crack tip in a cylindrical system. The Mode I and Mode II first terms on the bisector lead to a singular stress in the form of Eqs. (15) and (16):

$$\sigma_{\theta\theta}(\theta = 0) \propto K_I \, r^{1-\lambda_I} \tag{15}$$

$$\sigma_{r\theta}(\theta = 0) \propto K_{II} \, r^{1-\lambda_{II}} \tag{16}$$

where λ_I and λ_{II} are the singularity orders, which can take different values depending on the geometry. They are analytically determined for each configuration; more details can be found in (Barber, 2010). The singularity order is comparable for a close crack and an incomplete contact because of the tangency of both surfaces in contact, so $\lambda_I = \lambda_{II} = \frac{1}{2}$. In this single case, the shear intensity is directly linked to K_{II}:

$$K_T \propto K_{II} \tag{17}$$

The results from works on cracks subjected to combined loading have shown that the direct tensile loading, mode I, is the most critical on crack propagation followed by the in plane shear, Mode II, and by the out of plane shear, Mode III (Pook, 1994). The loading part that leads to a crack extension is the effective part of the loading, (Newman, 1984). In a first approach the effective part is the positive component of the loading range ΔK^{eff}.

If $K^{min} < 0$:

$$\Delta K^{eff} = K^{max} \tag{18}$$

If $K^{max} < 0$:

$$\Delta K^{eff} = 0 \tag{19}$$

If $K^{min} > 0$:

$$\Delta K^{eff} = \Delta K \tag{20}$$

6. Criterion construction

So as to propose a fretting crack initiation criterion, the different elements that have been introduced in the previous steps are used to correlate the experimental fretting crack thresholds with the materials properties. In a first approach, the goal is to propose a plain fretting criterion that can be applicable to different geometries. Then, an approach using Goodman's relationship and contact mechanics properties is used to show the evolution of the severity in the presence of bulk stress. Finally, those two approaches are combined to give a general fretting fatigue crack nucleation criterion.

6.1 Plain Fretting

By considering the contact edge as a crack in a homogeneous half-space, the plain fretting configuration becomes similar to a crack subjected to a mode II loading. Crack propagation in fatigue happens when the load is sufficient to open the crack. Newman et al. (Newman, 1984) proposed a relationship to determine the effort needed to open a crack when residual stresses exist at the singularity. The extension of the crack length produces a rise in the residual stress at the crack tip. The stress intensity factor range needed for a crack to propagate increases. In the same time, the friction between the crack lips can limit the stress intensity factor range available to open the crack. Those two phenomena limit the opening of the crack lips (Maierhofer, et al., 2014).

In the case of fretting contact, the mode I loading is negative so that the mode I has no influence on the crack initiation process. The plain fretting configuration is therefore similar to a mode II loading at the contact edge. By considering a tiny radius at the contact edge of the complete contact, all the geometries present singularity order $\lambda = 0.5$ allowing the comparison between each of them.

The alternate tangential loading of an incomplete contact leads to the existence of a partial slip and a stick zone. The partial slip zone can be seen as a pre-crack in a homogenous media loaded with a mode II loading. A significant part of the loading thus vanishes by friction at the interface. Figure 10 represents the evolution of the

shear intensity parameter ΔK_T^{eff} at the contact edge versus the size of the partial slip zone.
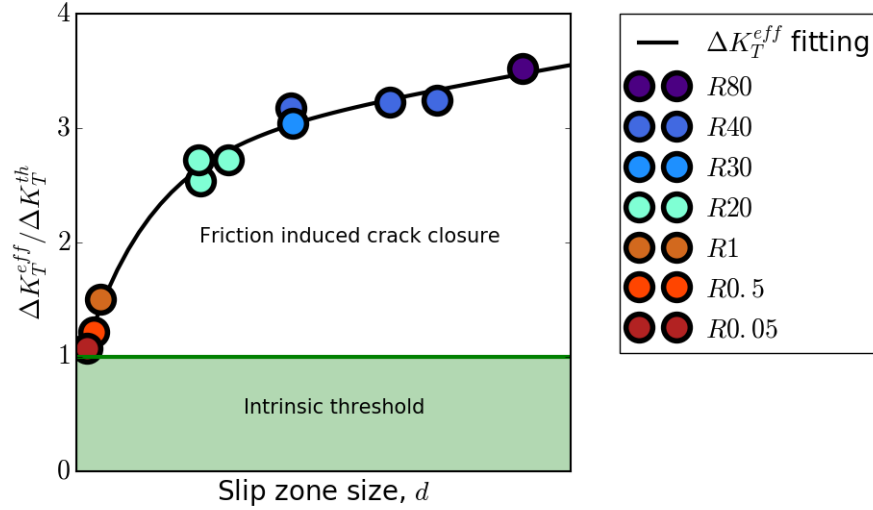

Figure 10 : Effective part of the shear intensity factor leading to a crack nucleation as a function of the slip zone size

This representation of the plain fretting tests is quite similar to the illustration of mode I crack propagation tests from Maierhoffer et al. (Maierhofer, et al., 2014). For a small crack, not subjected to crack closure phenomena, the complete load is used to extend the crack.

In the case shown in Figure 10, the fretting crack nucleation appears in almost complete contact ($R_{0.05}$) with very low shear intensity factors. The incomplete contacts are associated with larger slip zone size dominated by friction. The shear stress intensity needs to overcome the frictional threshold before nucleating a crack. From the representation of the shear stress intensity factor K_T in Figure 10, a shear stress intensity factor threshold exists and should be linked to an intrinsic material property.

Using the asymptotic fretting map representation, in a $\Delta K_T \times K_N$ space, when K_N tends to be infinite, ΔK_T^{eff} tends to this same intrinsic threshold. The results from (Churchman, et al., 2006) and (Karuppanan, et al., 2008) show that a critical coefficient of friction exists where no slip can occur at the edge of a complete contact. This coefficient of friction is $f = 0.543$ for a complete contact, producing a notch angle $\frac{\pi}{2}$ in alternate loading. For the Ti-10V-2Fe-3Al titanium alloy, the coefficient of

friction is $f = 0.84$ from (Hérédia, et al., 2011). The perfectly complete contact in fretting should therefore behave as a notch in a half-space. In this case, the fretting crack nucleation is supposed to appear when the loading overcomes the material crack propagation threshold, ΔK^{th} .
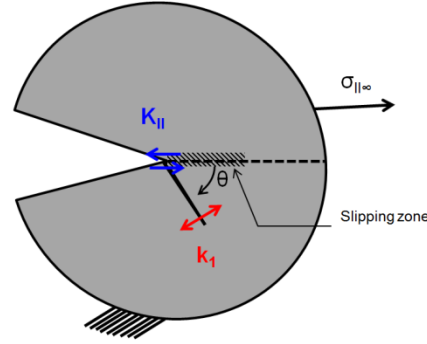

Figure 11 : Mode II loading at the contact edge of a complete contact and analogy with a notch in a half-space

The K_N parameter for a complete contact is considered as infinite because of the presence of a geometrical discontinuity. In this case the contact edge is analogue to a notch, represented in Figure 11. It is then possible to estimate stress intensity factor thresholds in mode II to nucleate a fretting crack from the crack propagation threshold in mode I as described by (Amestoy, et al., 1992).

This threshold, expressed in K_T dimensions, is shown in Figure 12 as the vertical asymptote of the plain fretting crack nucleation threshold, in green. $\Delta K_T{}^{th}$ is assumed to be the minimum value for a crack to nucleate at the singularity location.

By using the crack propagation threshold material property, the cracks are supposed to behave as mechanically short cracks whereas their lengths are about a few microns. Fretting cracks, as displayed in Figure 3, are propagating without any influence of the microstructure on the propagation path. This kind of propagation is representative of mechanically short crack propagation (Suresh, et al., 1984). From a continuum mechanics argument, there is a material intrinsic crack size, a_0, above which the crack propagation is considered to be consistent with linear elastic fracture mechanics (Tanaka, et al., 1981). In the application on Ti-10V-2Fe-3Al, the experimental crack nucleation threshold is greater than the intrinsic crack size ($5\mu m \gg a_0$).
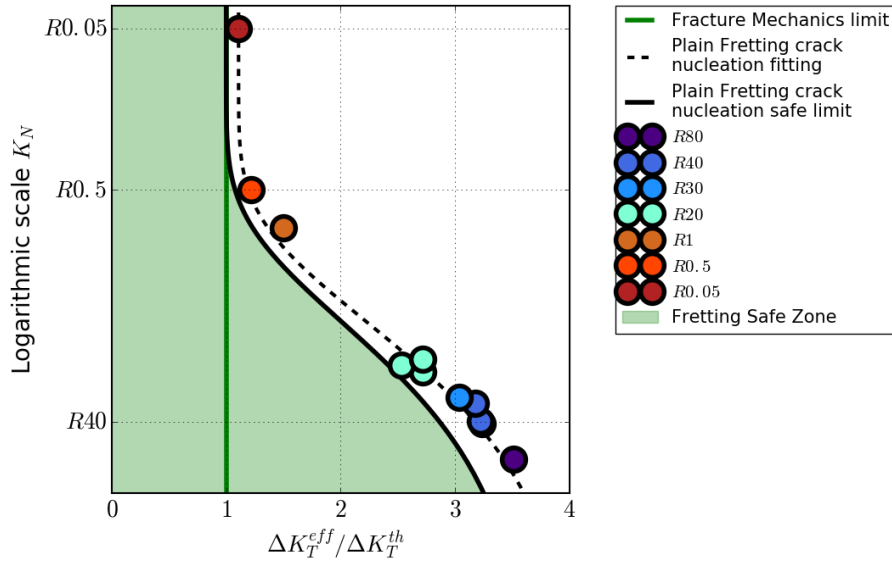
Figure 12 : Plain fretting crack nucleation prediction

To generalize the crack nucleation prediction to all geometries, a fitting parameter α is added. The fitting curve of all the plain fretting crack nucleation thresholds, represented in discontinuous line in Figure 12, is determined through Eq. (21).

$$\Delta K_T^{eff} = \Delta K_T^{R0.05}(1 + e^{1-\alpha K_N}) \tag{21}$$

Then, the safe limit is determined using the linear elastic fracture mechanic asymptote and the α parameter, by substituting $\Delta K_T^{R0.05}$ by ΔK_T^{th}. This safe limit is represented in Figure 12 by the black line at the boundary between the fretting crack safe zone and the fretting crack nucleation zone.

Equation (21) can be used as a plain fretting criterion for complete and incomplete contacts. The hypothesis on the materials behaviour is that they behave mainly as elastic fragile materials with a nucleation crack length threshold greater than the material intrinsic crack length a_0 (Tanaka, et al., 1981). The condition on the contact is to exhibit a coefficient of friction greater than the critical coefficient of friction from (Karuppanan, et al., 2008) and (Churchman, et al., 2006).

The main result of this analogy with linear elastic fracture mechanics is that a contact subjected to a sufficient normal loading to avoid any edge separation can behave as a notch in a homogeneous half-space. The case of complete contact is dominant in industrial assemblies. In this case, the fitting parameter, α, is not needed and the safe loading conditions can be determined from classical material properties only.

27

6.2 Fretting Fatigue

In presence of fretting fatigue, the shear stress at the interface is not anymore the only parameter leading to failure. The stress state in the bulk is leading to changes in the admissible stress. The conventional fatigue criteria use the hydrostatic pressure to consider this parameter. In the presence of static stress in the bulk the admissible stress in fatigue is lower than expected. In a uniaxial state of stress, this phenomenon can be handled using the Goodman relationship.

In plane strain conditions, the contact mechanics stress fields show a sharp stress gradient at the hot spot location. In this condition, the fretting contact can be considered as a uniaxial problem. Each of the stress components around the contact edge depend on K_N, as shown by Eqs. (11) and (12). K_N appears to be the parameter linked to the stress gradient at the contact edge. When the geometrical discontinuity becomes sharper, the K_N value increases and the volume subjected to a high level of stress decreases. (Papadopoulos, 1996) has shown that the fatigue limit in alternate bending test depends on the stress gradient. If the volume subjected to high stress is small, statistically the presence of defects is small and the admissible stress in fatigue is high (Hild, 1992).

As shown in Figure 9, the maximum stress at the trailing edge from a contact mechanics model depends on K_N. The concept of various fatigue stress limit, depending on the stress gradient, is comparable to Papadopoulos work (Papadopoulos, 1996). By using Eq. (13) on several fretting crack nucleation and splitting the alternating, or dynamic part, $\sigma_1{}^{dyn}$ and static $\sigma_1{}^{stat}$ part, it becomes possible to plot them on a Goodman diagram, see Figure 13.

In this figure, plain fatigue test results are also shown, illustrating how the Ti-10V-2Fe-3Al behaviour is consistent with the Goodman law:

$$\sigma_1{}^{dyn} = \sigma_f - \frac{\sigma_f}{R_m}\sigma_1{}^{stat} \tag{22}$$
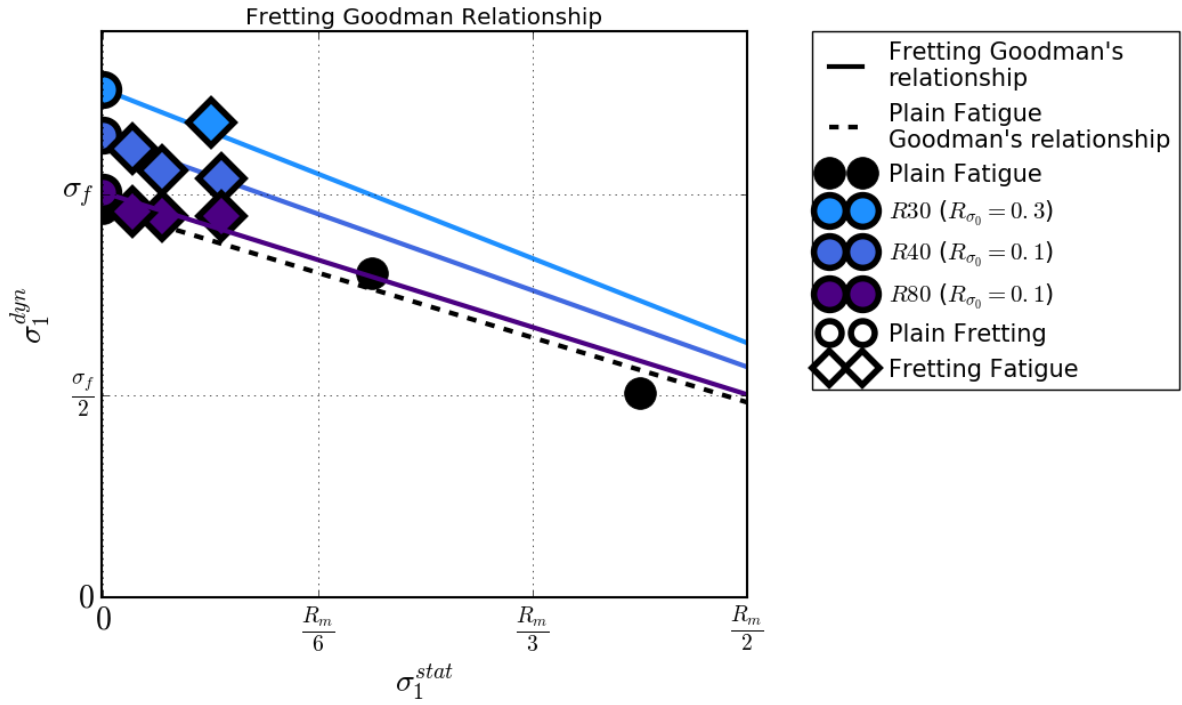
Figure 13 : Goodman's law applied to ICFN thresholds

The proposal here is to decompose the stress gradient at the contact edge into the different loadings contributions, as shown in Figure 14. The goal is to determine the tangential intensity factor K_T leading to the crack nucleation from the bulk-stress loading and its load ratio.
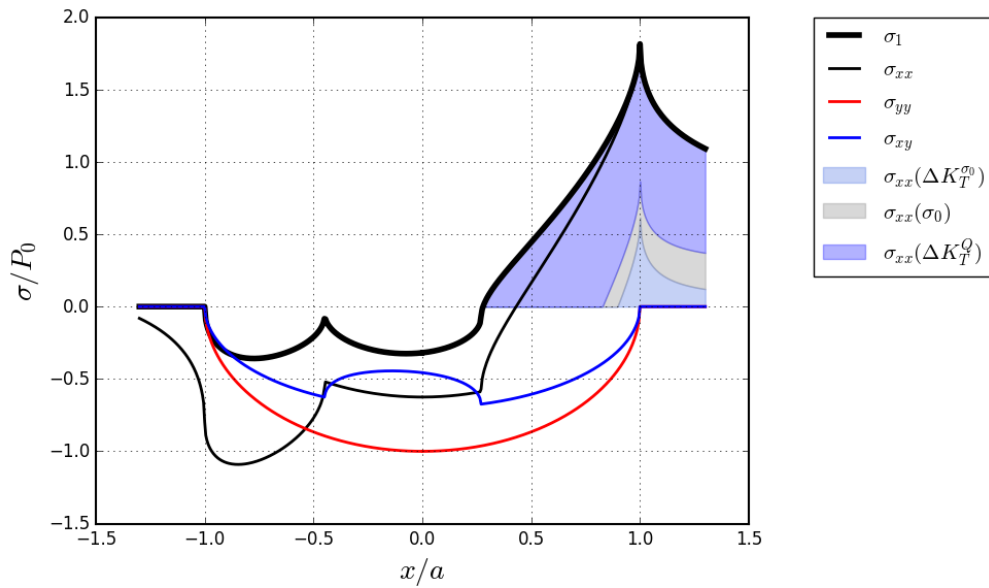

Figure 14 : Fretting fatigue trailing edge stress gradient decomposition from the different loadings for cylinder vs plane contact

In Figure 14, the trailing edge stress gradient at the critical loading is decomposed into three parts. The grey part is the bulk stress. This part is constant in the entire specimen, at the interface and in the bulk. The light blue area is the trailing edge stress gradient produced by the mismatch in strain following the bulk-stress application. The blue area is the trailing stress gradient generated by the tangential displacement from the pad on the plane.

The bulk stress applied to the specimen is composed of a static and an alternating part. The relation between both is expressed by the Eq. (23).

$$\sigma_0{}^{dyn} = \frac{(1 - R_{\sigma_0})}{(1 + R_{\sigma_0})} \sigma_0{}^{stat} \tag{23}$$

With a bulk stress ratio $R_{\sigma_0} = 0.1$, the admissible alternating stress is represented by the intersection of Eq. (22) and Eq. (23), displayed as the Plain Fatigue Failure point in the Goodman diagram, see Figure 15. This point represents the admissible loading in fatigue that can be applied on a dog bone specimen without any contact.
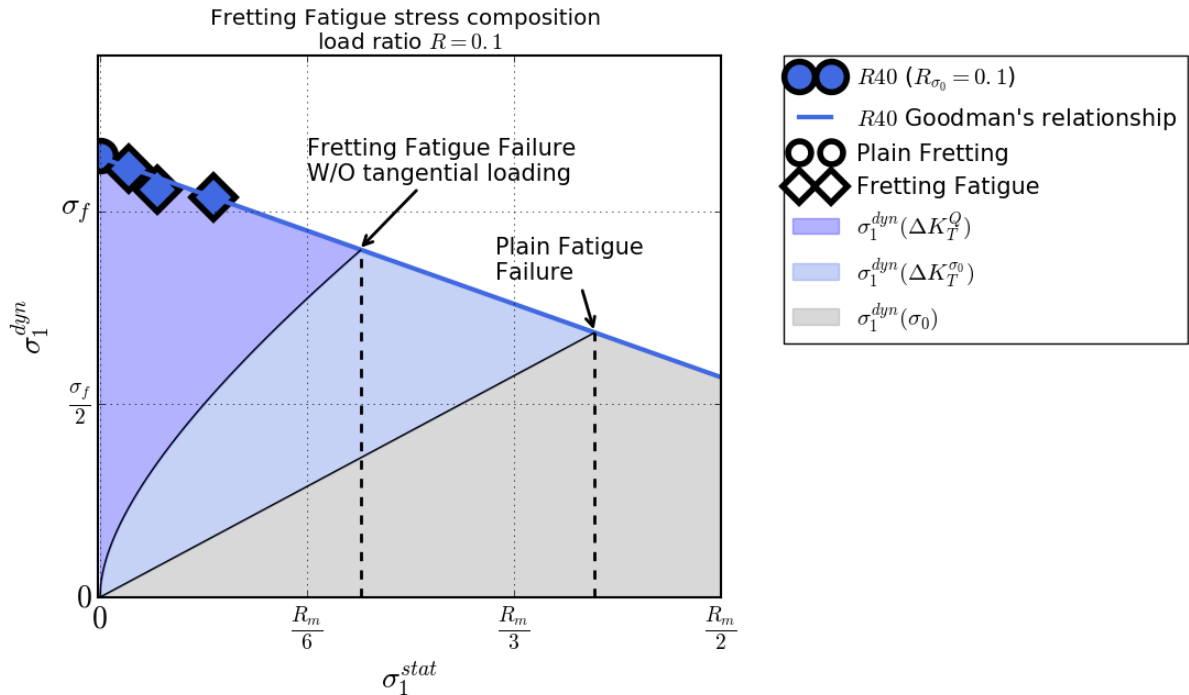

Figure 15 : Goodman diagram decomposition from incomplete contact with $R_Q = -1$ and $R_{\sigma_0} = 0.1$

In the presence of the contact, the alternating bulk stress leads to an extension of the slip zone. This is producing a rise in the trailing edge stress gradient, see Eq. (13). The failure is predicted to happen without tangential loading when the sum of the alternating bulk-stress and the trailing edge stress gradient overcome the Goodman relationship. This point is represented in Figure 15 by the fretting fatigue failure without tangential loading point. By substituting the different stress produced by the bulk-stress in the Goodman diagram, it is possible to determine the admissible tangential load to be applied on the pad to nucleate a fretting fatigue crack.

The main hypothesis behind this stress decomposition is that the shear stress produced by the alternating part of the bulk-stress leads to a small disruption of the slip zone size. This validity condition is expressed by Eq. (24). This expression from Hills *et al*. (Hills, et al., 1988), allows assuming the influence of the mismatch in strain as an offset on the stick zone location.

$$\frac{\sigma_0^{dyn}}{fP_0} < 4\left(1 - \sqrt{1 - \frac{Q}{fP}}\right) \tag{24}$$

Equation (24) can be rewritten using the asymptotic parameters, as Eq. (25). This condition of validity of the stress decomposition is illustrated in Figure 16 by the vertical red lines.

$$\Delta K_T^{\sigma_0} < \Delta K_T^Q \tag{25}$$

By substituting Eqs. (13) and (23) into the Goodman relationship (Eq. (22)), the tangential stress intensity factor in fretting fatigue leading to the crack nucleation can be expressed as Eq. (26).

$$\Delta K_T^{th,FF} = \frac{\left[\sqrt{4fK_N\Delta K_T^{th,PF}} - \left(\frac{\sqrt{4fK_N\Delta K_T^{th,PF}}}{R_m} + \frac{\left(1 - R_{\sigma_0}\right)}{\left(1 + R_{\sigma_0}\right)}\right)\sigma_0^{stat}\right]^2}{4fK_N} \tag{26}$$

The application of Eq. (26) is done with different cases of loading corresponding to fretting fatigue tests in Figure 16. In this same illustration, plain fretting and fretting fatigue crack nucleation contacts are plotted. In industrial applications, K_N tends to be infinite leading to a sharp notch configuration. In this case, the crack nucleation risk in

fretting fatigue does not depend anymore on the loading ratio but only on the intrinsic crack propagation threshold and the ultimate stress, R_m. The industrial safe zone represented by the green area in Figure 16, is the loading area where a complete contact subjected to a bulk stress ratio $R_{\sigma_0} = 0.3$ can unlikely occurs following the previous development.
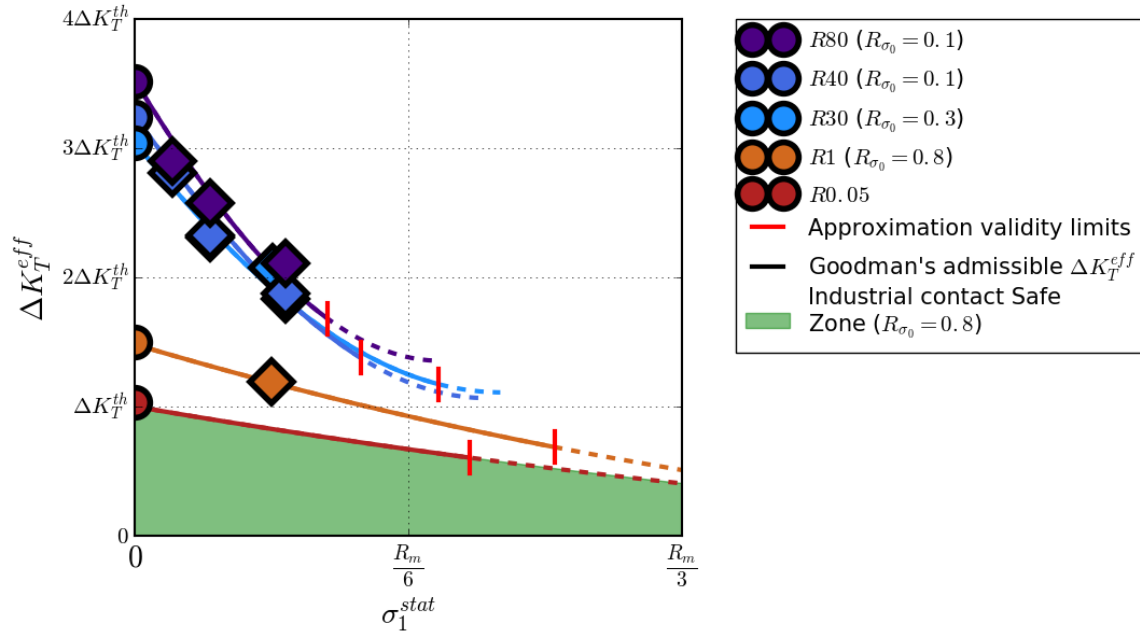

Figure 16 : Application of Goodman relationship to determine the loadings so as to nucleate a fretting fatigue crack

In presence of a material that follows the Goodman law as the Ti-10V-2Fe-3Al titanium alloy, Eq. (26) is a very efficient method to estimate the tangential load to nucleate a crack in fretting fatigue condition. A good correlation is observed between the thresholds determined experimentally and the proposed relation. Furthermore Eq. (26) does not require any additional parameter apart from classical material properties.

The evolution of the admissible tangential stress intensity factor with the increase of the bulk-stress is quite different depending on the geometries used. The cause of this change in behaviour in presence of bulk-stress could be linked to the volume subjected to the stress gradient. Indeed, with sharp edge contact, the bulk stress value is negligible compared to the stress gradient maximum stress.

6.3 Criterion Determination

In the two previous paragraphs, two fretting crack nucleation prediction methods have been proposed. The first one corresponds to plain fretting nucleation using an analogy with linear elastic fracture mechanics. The second one, in fretting fatigue configuration, uses the contact mechanics together with the Goodman relationship to find the crack nucleation conditions. By combining the two previous limits, a fretting fatigue criterion that can be used in plain fretting and fretting fatigue with several contact geometries from incomplete to complete contacts can be determined. This fretting criterion d_{FF} is expressed by Eq. (27) and takes a value higher than one when a crack nucleation is supposed to occur, here at 10^6 cycles. Equation (27) has been built by substituting Eq. (21) into Eq. (26).

$$d_{FF} = \frac{\Delta K_T{}^{eff}}{\left(\sqrt{\Delta K_T{}^{th} \left(1 + e^{(1-\alpha K_N)}\right)} - \frac{\sigma_0{}^{stat}}{R_m} \sqrt{\Delta K_T{}^{th} \left(1 + e^{(1-\alpha K_N)}\right)} - \frac{\left(1 - R_{\sigma_0}\right)}{\left(1 + R_{\sigma_0}\right)} \frac{\sigma_0{}^{stat}}{\sqrt{4 f K_N}} \right)^2} \quad (27)$$

This criterion compares the effective tangential stress intensity with the severity of the configuration composed by three terms. The first one corresponds to the stress gradient at the trailing contact edge; the second one accounts for the influence of the static part of the bulk-stress while the last one introduces the alternating bulk stress in the specimen.
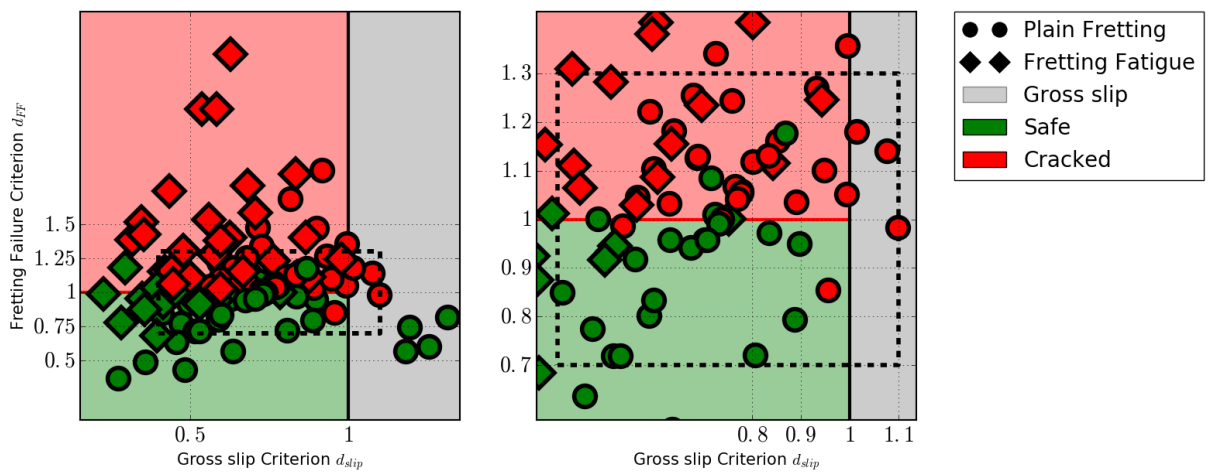

Figure 17 : Fretting criterion application on Ti-10V-2Fe-3Al complete, almost complete and incomplete fretting contact at 10^6 cycles

The application of the fretting criterion to all 136 fretting tests at 10^6 cycles, performed on Ti-10V-2Fe-3Al, allows a good prediction of the fretting crack nucleation. They are represented in Figure 17, showing three different coloured areas. The grey one is the gross slip zone determined by the gross slip criterion, Eq. (9). The red one is the area where the contact configuration can lead to a crack nucleation at 10^6 cycles. The green one is the safe crack nucleation area, which is bounded by the fretting crack nucleation criterion, Eq. (27).

7. Conclusion

The use of the contact eigenvalues allows describing the global behaviour of the contact leading to fretting crack initiation. The increase of normal load and the stress concentration with discontinuous contact geometries decrease drastically the admissible tangential stress intensity at the contact edge. The plain fretting crack nucleation has been considered through an analogy with linear elastic mechanics that allows using classical material properties. The presence of bulk-stress in one of the contacting part produces two kinds of stresses: it contributes to the shear stress because of the mismatch in strain that is included in ΔK_T^{eff} parameter and to the presence of the bulk-stress in the specimen. The static part of this bulk-stress reduces the admissible alternating stress at the hotspot location. The prediction of this contribution has been performed with the Goodman relationship (Goodman, 1899). The combination of those two approaches leads to the proposal of an efficient fretting fatigue criterion. This criterion allows to determine a safe zone under both plain fretting and fretting fatigue at 10^6 cycles. When considering complete contact configurations, it does not require any calibration process and uses only classical material parameters (ΔK_{th} and R_m). For a generalization to any contact geometry, only one calibration parameter is necessary. This criterion has been successfully applied to predict the crack nucleation risks for fretting tests between Ti-10V-2Fe-3Al titanium alloy parts with various geometries and over a wide range of load levels.

A great interest when using asymptotic parameters is to reflect a non-local state of stress. This kind of approach is helpful for many industrial applications as the non-local methods are less dependent on mesh refinement. The use of this asymptotic

criterion will be evaluated on industrial assemblies to perform efficient and reliable fretting crack risk estimation.

8. Acknowledgements

9. Bibliography

Amargier, R. 2011. Amorçage de fissures et gradient de contraintes en fretting et en fatigue. *Ph.D thesis.* Ecole Centrale de Lyon, 2011.

Amestoy, M. and Leblond, J. 1992. Crack paths in plane situations – II. Detailed form of the expansion of the stress intensity factors. *International Journal of Solids and Structures.* 1992, Vol. 29, 465-501.

Andresen, H., et al. 2019. Frictional half-plane contact problems subject to alternating normal and shear loads and tension in the steady state. *International Journal of Solids and Structures.* 2019, Vol. 168, 166-171.

Baietto, M. C., Pierres, E. and Gravouil, A. 2010. A multi-model X-FEM strategy dedicated to frictional crack growth under cyclic fretting fatigue loadings. *International Journal of Solids and Structures.* 2010, Vol. 47, 10, pp. 1405-1423.

Baietto, M.C., et al. 2013. Fretting fatigue crack growth simulation based on a combined experimental and XFEM strategy. *International Journal of Fatigue.* 2013, Vol. 47, 31-43.

Barber, J.R. 2010. *Elasticity.* s.l. : Springer, 2010.

Blanchard, P. 1991. Usure induite en petits débattements: Transformation tribologique superficielle d'alliages de titane. *Ph.D thesis.* Ecole Centrale de Lyon, 1991.

Cattaneo, C. 1938. Sui contatto di due corpi elastici; distribuzione locale degli sforzi. *Rendiconti dell' Accademia nazionale dei Lincei.* 1938, Vol. 27, 342-348, 434-436, 474-478.

Churchman, C. and Hills, D.A. 2006. General results for complete contacts subjects to oscillatory shear. *Journal of the Mechanics and Physics Solids.* 2006, Vol. 22, 1186-1205.

Ciavarella, M. 1998b. The generalized Cattaneo partial slip plane contact problem II-examples. *International Journal of Solids and Structures.* 1998b, Vol. 35, 2349-2362.

—. **1998a.** The generalized Cattaneo partial slip plane contact problem I-theroy. *International Journal of Solids and Structures.* 1998a, Vol. 35, 2363-2378.

Dini, D. and Hills, D.A. 2004. Bounded Asymptotic solutions for incomplete contacts in partial slip. *International Journal of Solids and Structures.* 2004, Vol. 41, 7049-7062.

Dundurs, J. 1969. Discussion of edge-bonded dissimilar othogonal elastic wedges under normal and shear loading. *Journal of Applied Mechanics.* 1969, Vol. 36, 650-652.

Fellows, L.J., Nowell, D. and Hills, D.A. 1997. On the initiation of fretting fatigue cracks. *Wear.* 1997, Vol. 205, 120-129.

Ferre, R., et al. 2013. Prediction of the Fretting Fatigue Crack nucleation endurance of a Ti-6V-4Al/Ti-6V-4Al interface: Influence of plasticity and tensile/shear fatigue properties. *Procedia Engineering.* 2013, Vol. 66, 803-812.

Fleury, R.M.N, Hills, D.A. and Barber, J.R. 2016. A corrective solution for finding the effects of edge-rounding on complete contact between elastically similar bodies. Part II: Near-edge asymptotes and the effect of shear. *International Journal of Solids and Structures.* 2016, Vols. 85-86, 97-104.

Flicek, R., Hills, D.A. and Dini, D. 2013. Progress in the application of notch asymptotics to the understanding of complete contacts subject to fretting fatigue. *Fatigue and Fracture of Engineering Materials and Structures.* 2013, Vol. 36, 56-64.

Fouvry, S., et al. 1998. Identification of the characteristic length scale for fatigue cracking in fretting contacts. *Le journal de Physique IV.* 1998, Vol. 8, 159-166.

Fouvry, S., et al. 1996. Theorical analysis of fatigue cracking under dry friction for fretting loading conditions. *Wear.* 1996, Vol. 195, 21-34.

Fridrici, V., et al. 2005. Prediction of cracking in Ti-6Al-4V alloy under fretting wear: use of the SWT criterion. *Wear.* 2005, Vol. 259, 2000-2005.

Giannakopoulos, A.E., Lindley, T.C. and Suresh, S. 1998. Aspect of equivalence between contact mechanics and fracture mechanics: theorical connections and life prediction methodology for fretting fatigue. *Acta Materiala.* 1998, Vol. 46, 2955-2968.

Goodman, J. 1899. *Mechanics Applied to Engineering.* London : Longman Green, 1899.

Hérédia, S. 2012. Etude expérimentale et prédiction des conditions d'amorçage des fissures dans un assemblage rotor soumis à des chargements de fretting fatigue. *Ph.D thesis.* Ecole Centrale de Lyon, 2012.

Hérédia, S., et al. 2011. A non-local fatigue approach to quantify Ti-10V-2Fe-3Al fretting cracking process: Application to grinding and shot peening. *Tribology International.* 2011, Vol. 44, 1518-1525.

Hérédia, S., et al. 2014. Introduction of a "principal stress-weight function" approach to predict the crack nucleation risk under fretting fatigue using FEM modelling. *International Journal of Fatigue.* 2014, Vol. 61, 191-201.

Hertz, H. 1882. Ueber die Beruehrung fester elasticher Koerper. *J. reine und angewandte Mathematik.* 1882, Vol. 92, 156-171.

Hild, F. 1992. De la rupture des materiaux à comportement fragile. *Ph.D thesis.* Université Paris 6, 1992.

Hills, D.A. 1993. Contact Mechanics. 1993.

Hills, D.A., et al. 2017. A unified approach for representing fretting and damage at the edges of incomplete and receding contacts. *Tribology International.* 2017, Vol. 108, 16-22.

Hills, D.A., Fleury, R.M.N. and Dini, D. 2016. Partial slip incomplete contacts under constant normal load and subject to periodic loading. *International Journal of Mechanical Science.* 2016, Vols. 108-109, 115-121.

Hills, D.A., Nowell, D. and O'Connor, J.J. 1988. On the mechanics of fretting fatigue. *Wear.* 1988, Vol. 125, 129-146.

Hutson, A.L., Ashbaugh, N.E. and Nicholas, T. 2003. An Investigation of Fretting Fatigue Crack Nucleation Life of Ti-6Al-4V under Flat-on-Flat Contact. *Fretting Fatigue: Advances in Basic Understanding and Applications.* ASTM International, 2003, 307-322.

Jäger, J. 1997. Half-planes without coupling under contact loading. *Archive of Applied Mechanics.* 1997, Vol. 67, 247-259.

Karuppanan, S. and Hills, D.A. 2008. Frictional complete contacts between elastically similar bodies subject to normal and shear load. *International Journal of Solids and Structures.* 2008, Vol. 45, 4662-4675.

Kubiak, K., Fouvry, S. and Marechal, A. 2005. A practical methodology to select fretting palliatives: Application to shot peening, hard chromium and WC-Co coatings. *Wear.* 2005, Vol. 259, 367-376.

Lamacq, V. and Dubourg, M-C. 1999. Modelling of initial fatigue crack growth and crack branching under fretting conditions. *Fatigue & Fracture of engineering materials ans structures.* 1999, Vol. 22, 535-542.

Lamacq, V., Dubourg, M.C. and Vincent, L. 1996. Crack Path Prediction Under Fretting Fatigue - A theoretical and Experimental Approach. *Journal of Tribology.* 1996, Vol. 118, 711-720.

Lamacq, V., Dubourg, M-C. and Vincent, L. 1997. A theorical model for the prediction of initial crack growth angles and sites of fretting fatigue cracks. *Tribology International.* 1997, Vol. 30, 391-400.

Lee, H. and Mall, S. 2006. Investigation into effects and interaction of various fretting fatigue variables under slip-controlled mode. *Tribology International.* 2006, Vol. 39, 1213-1219.

Lykins, C.D., Mall, S. and Jain, V.K. 2001. Combined experimental-numerical investigation of fretting fatigue crack initation. *International Journal of Fatigue.* 2001, Vol. 23, 703-711.

Maierhofer, J., Pipnan, R. and Ganser, R.P. 2014. Modified NASGRO equation for physically short cracks. *International Journal of Fatigue.* 2014, Vol. 59, 200-207.

Mall, S., et al. 2003. Fretting Fatigue Crack Initiation Behavior of Ti-6Al-4V. *Fretting Fatigue: Advances in Basic Understanding and Applications.* ASTM International, 2003, 338-352.

Meriaux, J., et al. 2010. Characterization of crack nucleation in TA6V under fretting-fatigue loading using the potential drop technique. *International Journal of Fatigue.* 2010, Vol. 32, 1658-1668.

Mindlin, R.D. 1949. Compliance of elastic bodies in contact. *Journal of Applied Mechanics.* 1949, Vol. 16, 259-268.

Montebello, M.C. 2015. Analysis of the stress gradienteffect in fretting-fatigue through a description based on non-local intensity factors. *Ph.D thesis.* Université Paris-Saclay, 2015.

Mugadu, A., et al. 2004. The application of asymptotic solutions to characterising the process zone in almost complete frictional contacts. *International Journal of Solids and Structures.* 2004, Vol. 41, 1333-1346.

Muskhelishvili, N.I. 1953. *Some Basic Problems of the Mathematical Theory of Elasticity.* Gröningen : Noordhoff, 1953.

Naboulsi, S. 2005. Applications of crack analogy to fretting fatigue. *Engineering Fracture Mechanics.* 2005, Vol. 72, 1610-1623.

Newman, J.C. 1984. A crack opening stress equation for fatigue crack growth. *International Journal of Fracture.* 1984, Vol. 24, 131-135.

Nowell, D. 1988. An analysis of fretting fatigue. *Ph.D thesis.* University of Oxford, 1988.

Papadopoulos, I.V. 1996. Invariant formulation of a gradient dependent multiaxial high-cycle fatigue criterion. *Engineering Fracture Mechanics.* 1996, Vol. 55, 513-528.

Pook, L.P. 1994. Mixed Mode Fatigue Crack Propagation. *Handbook of Fatigue Crack Propagation in Metallic Structures.* Carpinteri, A.,, 1994.

Proudhon, H., Fouvry, S. and Buffière, J.Y. 2005. A fretting crack initiation prediction taking into account the surface roughness and the crack nucleation process volume. *International Journal of Fatigue.* 2005, Vol. 27, 569-579.

Suresh, S. and Ritchie, R.O. 1984. Propagation of short fatigue cracks. *International Metals Reviews.* 1984, Vol. 29, 445-475.

Szolwinski, M.P and Farris, T.N. 1998. Observation analysis and prediction of fretting fatigue in 2024-T351 aluminium alloy. *Wear.* 1998, Vol. 221, 24-36.

Tanaka, S., Nakai, Y. and Yamashita, M. 1981. Fatigue growth threshold of small cracks. *International Journal of Fracture.* 1981, Vol. 17, 519-533.

Vincent, L., et al. 1992. Mechanics and materials in fretting. *Wear.* 1992, 135-148, pp. 135-148.

Williams, M. 1956. On the stress distribution at the base of a stationary crack. *Journal of Applied Mechanics.* 1956, Vol. 24, 109-114.